State selected ion–molecule reactions by a TESICO technique. II. Separation of the reactant spin–orbit states in the reaction Ar+(2 P 3/2, 2 P 1/2)+H2(D2)→ArH+(ArD+)+H(D)

Kenichiro Tanaka, Jean Durup, Tatsuhisa Kato, and Inosuke Koyano

Citation: The Journal of Chemical Physics **74**, 5561 (1981); doi: 10.1063/1.440919
View online: http://dx.doi.org/10.1063/1.440919
View Table of Contents: http://scitation.aip.org/content/aip/journal/jcp/74/10?ver=pdfcov
Published by the AIP Publishing

State selected ion–molecule reactions by a TESICO technique. II. Separation of the reactant spin–orbit states in the reaction $Ar^+(^2P_{3/2}, ^2P_{1/2})+H_2(D_2)\rightarrow ArH^+(ArD^+)+H(D)$

Kenichiro Tanaka, Jean Durup,[a] Tatsuhisa Kato, and Inosuke Koyano

Institute for Molecular Science, Myodaiji, Okazaki, 444 Japan
(Received 10 December 1980; accepted 22 January 1981)

Cross sections for the atomic rearrangement reaction $Ar^+ + H_2(D_2)\rightarrow ArH^+(ArD^+) + H(D)$ [Reaction (1)] and the charge transfer reaction $Ar^+ + H_2(D_2)\rightarrow Ar + H_2^+(D_2^+)$ [Reaction (2)] have been determined for each of the Ar^+ spin–orbit states ($^2P_{3/2}$ and $^2P_{1/2}$) separately in the collision energy range from 0.05 to 0.5 eV (c.m.), utilizing the threshold electron–secondary ion coincidence (TESICO) technique which we developed recently. It has been found that the cross sections of Reaction (1) are larger for the $^2P_{1/2}$ excited state than for the $^2P_{3/2}$ ground state by a factor of 1.5 (with H_2) and 1.3 (with D_2), regardless of the collision energy in the range studied. The cross sections for both the H_2 and D_2 reactions show an approximately $E^{-1/2.5}$ collision energy dependence which is somewhat milder than that expected from the simple Langevin theory. The cross sections of Reaction (2) have been found to be about seven times larger for the $^2P_{1/2}$ state than for the $^2P_{3/2}$ state with H_2, whereas these are almost the same for both states with D_2. The charge transfer cross sections are almost independent of the collision energy in the same energy range as above. A simple reaction model has been developed and a calculation of cross sections has been performed based on it, with a result which satisfactorily explains the essential features of the experimental results.

I. INTRODUCTION

The importance of the concept of nonadiabatic transitions between two adiabatic potential energy surfaces in understanding many physical and chemical processes has increasingly been recognized in recent years.[1] Prototypes of such processes include collisional quenching of electronically excited atoms and molecules, electronic excitation in collisions of vibrationally or translationally excited molecules, charge transfer, internal conversion in polyatomic molecules, and some chemical (rearrangement) reactions.

Ion–molecule reactions constitute a unique class of chemical reactions involving such nonadiabatic transitions owing to their very nature that, in most systems, charge transfer and molecular rearrangement compete. Apparently more than one adiabatic surface is needed to describe these two product channels.

From this viewpoint, the reaction $Ar^+ + H_2$ and its isotopic analog

$$Ar^+ + H_2(D_2) \rightarrow ArH^+(ArD^+) + H(D) \qquad (1)$$

have extensively been investigated theoretically.[2–4] These investigations have shown that while the diabatic picture is the best representation of this system in the two asymptotic regions $(Ar-H_2)^+$ and $(ArH-H)^+$ the electronic coupling of such diabatic states in between the two regions is essential for Reaction (1) and the charge transfer reaction

$$Ar^+ + H_2(D_2) \rightarrow Ar + H_2^+(D_2^+) \qquad (2)$$

to occur. This is because the ground state ArH^+ dissociates only into $Ar + H^+$ (not into $Ar^+ + H$) in this asymptotic region,[2] indicating that only the reactant state $Ar + H_2^+$ correlates with the ground state of $ArH^+ + H$.

The important coupling has been found to be localized in a small area of the configuration space in the entrance channel (large translational coordinate R), and the crossing seam to lie orthogonal to the H_2 vibrational coordinate. The latter fact indicates that the transitions are induced by the vibrational motion rather than by translational motion. From dynamical investigations using the 3D trajectory surface hopping model, the predictions for cross sections, average final translational energy, and average scattering angle have been obtained at one energy.[3] The results agree well with experiment.[5–9]

There exists, however, another complicating, but very intriguing factor with this system, viz., spin–orbit coupling. The reactant Ar^+ ion has doubly degenerate $^2P_{1/2}$ states 0.178 eV above the fourfold degenerate $^2P_{3/2}$ ground states. The spin–orbit coupling is of interest because of the two consequences it can have: Firstly, it may resolve otherwise degenerate potential energy surfaces in the asymptotic region, and, secondly, it may induce nonadiabatic transitions between surfaces. Although the importance of this coupling has often been emphasized, there has been no theoretical investigation which includes this effect explicitly.

Reaction (1) has also most extensively been studied experimentally. Various techniques, such as conventional mass spectrometers,[5,10–12] tandem mass spectrometers,[13,14] velocity analyzers (with and without angle analysis),[7,15–18] crossed beams with energy and angular distribution measurements,[6,19] flowing afterglows,[20] and ion cyclotron resonance,[21] have been applied with the results which are not in complete agreement. Charge transfer reaction (2),[9,22,23] as well as elastic[7] and inelastic[24] scattering of Ar^+ by H_2 have also been studied. Again, however, there has been no direct information on the effect of spin–orbit coupling.

Chupka and Russell[25] reported evidence for about a 1.3 times larger cross section of Reaction (1) (with H_2)

[a]IMS Invited Foreign Scholar, September–December, 1979. Permanent address: Laboratoire des Collisions Atomiques et Moleculaires, Université Paris-Sud, 91405 Orsay, France.

 0021-9606/81/105561-11$01.00

for the $^2P_{1/2}$ state than for the $^2P_{3/2}$ ground state at nominally zero kinetic energy. This value was deduced from the photoionization intensity curves obtained with a single ionization chamber and a mixture of Ar and H_2. Very recently, Rakshit and Warneck[26] interpreted their observation of "unusual" initial decay of the Ar^+ parent ions with H_2 pressure in a selected ion-drift chamber mass spectrometer as indicative of the fact that the excited $Ar^+(^2P_{1/2})$ ions are quenched very rapidly by H_2 but the reaction of them with H_2 is much slower than that of the ground state $Ar^+(^2P_{3/2})$ ions. They deduced from this decay data a quenching rate constant which is larger than the Langevin value and a reaction rate constant of the $^2P_{1/2}$ state which is about two orders of magnitude smaller than that of the $^2P_{3/2}$ state. They measure, however, only the overall Ar^+ intensities, and their interpretation and the deduction processes do not seem to be unequivocal.

We have recently performed a direct determination of the separate cross sections of Reaction (1) for the two states,[27] utilizing a threshold electron–secondary ion coincidence (TESICO) technique.[28] Preliminary results on the ratio of the reaction cross sections $\sigma(1/2)/\sigma(3/2)$ have been reported.[27] In the present paper, we present, after briefly reviewing the experimental technique in Sec. II, a complete report of the determination of the individual absolute cross sections for Reactions (1) and (2) in Sec. III. Results are also discussed in Sec. III. In addition, we have developed a theoretical model and carried out approximate calculations of cross sections based on it, with the results in fair agreement with the experiment. These are presented and discussed in Sec. IV.

II. EXPERIMENTAL

The TESICO technique and the apparatus (named TEPSICO) have been described in detail elsewhere[28] and are described here only briefly. In the present study, the double-chamber mode of operation, namely, the ion beam–gas chamber method was used, in contrast with previous studies. This avoided the ambiguity inherent to the single chamber experiments due to the simultaneous occurrence of more than one reactant ion (Ar^+ and H_2^+ in the Ar/H_2 system).

The reactant Ar^+ ions were produced in an ionization chamber by photoionization of Ar at threshold wavelengths of $Ar^+(^2P_{3/2})$ and $Ar^+(^2P_{1/2})$ (786.5 and 777.5 Å, respectively), the monochromatic light being supplied by a helium Hopfield continuum light source and a 1 m Seya-Namioka monochromator (0.52 A FWHM). The ions and photoelectrons were extracted from the ionization chamber in opposite directions to each other. The ions, after extraction, were formed into a beam of desired velocity and led into the reaction chamber which contains H_2 or D_2 gas. The product $ArH^+(ArD^+)$ ions, as well as unreacted primary Ar^+ ions, were extracted from the reaction chamber in the same direction as the primary ion beam, mass-analyzed by a quadrupole mass spectrometer, and detected by a channel multiplier. These ion signals were then counted in coincidence with the threshold photoelectron signals obtained with a hemispherical electrostatic electron energy analyzer.

The collision energies were determined by the potential difference between the position of the origin of the primary ions (center of the incident photon beam) and the reaction chamber. Since there is no potential gradient in the reaction chamber, the collision energy is defined much more precisely than with the single-chamber method where only the average collision energy is defined.

The intensity of the helium Hopfield continuum was improved over the previous work by a factor of more than 20 by the installation of an extremely high-power pulse generator (Velonex Model V-2403). This facilitated the present double-chamber experiments. The pressure of the He gas and the path length of discharge were the same as before.

Since the intensities of the product $H_2^+(D_2^+)$ ions of the charge transfer reactions (2) were extremely weak, the coincidence measurements were not practical with these ions. Instead, the product $H_2^+(D_2^+)$ ions were measured without coincidence at two wavelengths, 786.5 and 584 Å, with the latter wavelength (resonance line) being supplied by a low-pressure dc discharge through He. The procedure for obtaining charge transfer cross sections for each state from this measurements is given in the next section.

High-purity argon ($\geq 99.999\%$) and hydrogen (99.9999%) were obtained from the Japan Oxygen Co.

III. EXPERIMENTAL RESULTS AND DISCUSSION

A. Coincidence spectra of Ar^+ and ArH^+ with threshold electrons

A typical example of coincidence TOF spectra of the primary Ar^+ and secondary ArH^+ ions with threshold electrons is shown in Fig. 1. The spectra were taken at 777.5 Å [threshold wavelength for the $Ar^+(^2P_{1/2})$ excited state] and thus the detected ions correspond to $Ar^+(^2P_{1/2})$ and the ArH^+ ions produced from this reactant. The H_2 pressure in the reaction chamber, and the laboratory kinetic energy of Ar^+ were 3.2×10^{-3} torr and 1.5 eV, respectively. The overall resolution of the threshold electron analyzer of about 25 meV [see Fig. 3 in Ref. 28(b)] was used to obtain higher intensity, although the analyzer had been improved to attain a maximum resolution of 14.5 meV. The average count rates of the threshold electrons and the primary and secondary ions, and the signal accumulation time T required to obtain these spectra are given in the figure. The ordinates indicate the total number of coincidence counts obtained throughout the time T. The spectra show raw data without subtracting background.

B. State selected cross sections for the rearrangement channel

1. *Determination of cross sections*

The absolute cross sections for Reaction (1) for each spin–orbit state were determined as a function of collision energy. These were determined directly from the coincidence intensity ratio $(ArH^+)/(Ar^+)$ (ratio of the

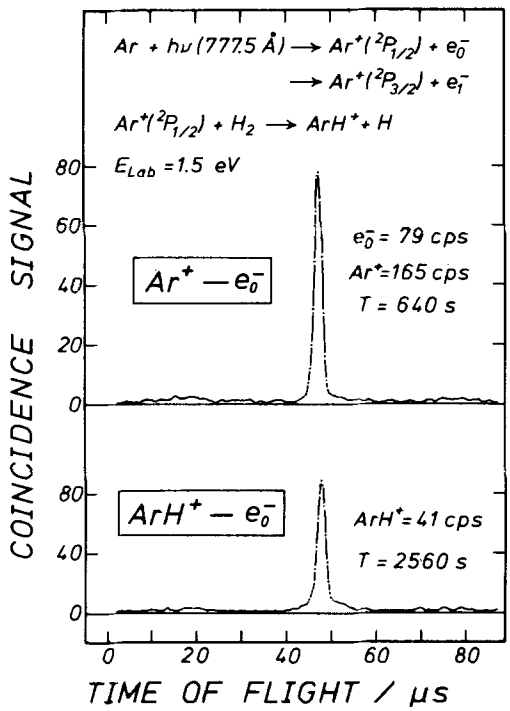

FIG. 1. Coincidence TOF spectrum of the primary (Ar^+) and secondary (ArH^+) ions of Reaction (1) with threshold photoelectrons (e_0^-). Incident wavelength was 777.5 Å, corresponding to the threshold for the $^2P_{1/2}$ excited state of Ar^+. T represents the signal accumulation time and the ordinates indicate number of coincidence counts obtained during respective T.

areas of the coincidence peaks) of the primary and secondary ions.

While the present double-chamber coincidence technique separates the two spin–orbit states clearly, there still exists general complexity inherent to the beam-chamber method. Thus, in determining the absolute cross sections for Reaction (1), the following reactions of $Ar^+ + H_2$ and subsequent reactions of the product ArH^+ and H_2^+ ions must be taken into account:

$$Ar^+ + H_2 \rightarrow ArH^+ + H\,, \quad \sigma_r\,, \tag{1}$$

$$\rightarrow Ar + H_2^+\,, \quad \sigma_t\,, \tag{2}$$

$$\rightarrow \text{scattering}\,, \quad \sigma_s\,; \tag{3}$$

$$ArH^+ + H_2 \rightarrow H_3^+ + Ar\,, \quad \sigma_r'\,, \tag{4}$$

$$\rightarrow \text{scattering}\,, \quad \sigma_s'\,; \tag{5}$$

$$H_2^+ + H_2 \rightarrow H_3^+ + H\,, \quad \sigma_r''\,, \tag{6}$$

$$\rightarrow \text{scattering}\,, \quad \sigma_s''\,; \tag{7}$$

$$H_3^+ + H_2 \rightarrow \text{scattering}\,, \quad \sigma_s'''\,. \tag{8}$$

Also, we have to consider the different collecting efficiencies for different ions. These are denoted by λ, λ', λ'', and λ''' for Ar^+, ArH^+, H_2^+, and H_3^+, respectively. Taking all these factors into consideration and solving rate equations for these reactions, we finally obtain the expression for σ_r (see Appendix A):

$$\sigma_r = \frac{\lambda}{\lambda'(m-q)nd} \ln\left[1 + (m-q)\frac{(ArH^+)}{(Ar^+)}\right], \tag{9}$$

where n is the number density of H_2, d is the reaction path length (thickness of the reaction chamber ≡ 0.6 cm), and m and q are given by

$$m = \lim_{n\to 0}\left[-\frac{d(Ar^+)}{d(ArH^+)}\right] \equiv \frac{\lambda}{\lambda'}\left(1 + \frac{\sigma_t + \sigma_s}{\sigma_r}\right), \tag{10}$$

$$q = \left[\frac{(Ar^+)}{(ArH^+)}\right]_\infty \equiv \frac{\lambda}{\lambda'} \cdot \frac{\sigma_r' + \sigma_s'}{\sigma_r}\,, \tag{11}$$

the suffix ∞ in the latter equation meaning that this is the value at $d(ArH^+)/d(Ar^+) = 0$. These constants are experimentally determinable as follows: As a result of Reactions (1)–(7), the observed intensities (Ar^+) and (ArH^+) vary with H_2 pressure in such a manner that, when (ArH^+) is plotted vs (Ar^+), (ArH^+) first increases, passes through a plateau, and then decreases as (Ar^+) decreases. This is illustrated in Fig. 2 for the case of the D_2 reaction measured at 786.6 Å [only $Ar^+(^2P_{3/2})$ is produced] and ion kinetic energy (LAB) of 1.0 eV. The ratio (Ar^+)/(ArH^+) at this plateau gives the value of q and the initial ($n \rightarrow 0$) slope of the curve gives the value of m, as shown in Fig. 2.

Using these constants, the procedure for determining the ratio λ/λ' (and hence σ_r) is as follows: First, the zeroth approximation ratios σ_t/σ_r and σ_s/σ_r are estimated, respectively, from the intensity ratio H_2^+/ArH^+ and the scattering experiments performed using He. With these ratios, λ/λ' is obtained from Eq. (10). This value, together with m and q, gives σ_r of first approximation according to Eq. (9). σ_r thus obtained modifies the estimated ratio σ_s/σ_r (the ratio σ_t/σ_r is constant irrespective of the absolute value of σ_r) and the new set of ratios is used in Eq. (10) to yield new λ/λ' and σ_r. This procedure is repeated until σ_r is not changed any more by this process.

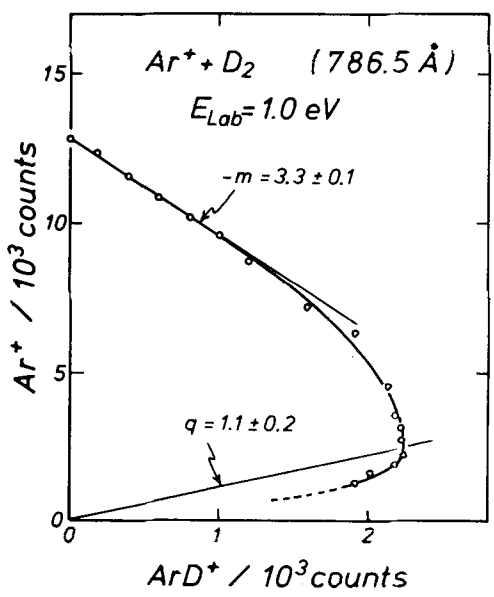

FIG. 2. Plot of secondary ion intensity vs primary ion intensity, showing the determination of m and q in Eq. (9). Each datum point corresponds to a pressure of D_2 in the reaction chamber.

2. Results and discussion

Experimental results are summarized in Fig. 3 which shows the cross sections for individual reactant states as a function of collision energy. From the figure, several interesting aspects are immediately evident: First, the cross section at a fixed collision energy is always larger for the $^2P_{1/2}$ excited state than for the $^2P_{3/2}$ ground state in both the H_2 and D_2 reactions. Second, however, the cross section ratio $\sigma(1/2)/\sigma(3/2)$ is larger for the H_2 reactions than for the D_2 reactions, namely, there is isotope effect in this ratio. Third, this ratio is independent of collision energy within the range studied here (0.05–0.50 eV c.m.) and is about 1.5 for the H_2 reactions and about 1.3 for the D_2 reactions. Finally, the cross sections show somewhat less steep collision energy dependences than that expected from the simple Langevin theory ($E^{-1/2.3}$ and $E^{-1/2.6}$ dependences for the H_2 and D_2 reactions, respectively).

Although Reaction (1) is one of the most extensively studied of all ion–molecule reactions, there has been no direct information on the reactivity of individual spin–orbit states of Ar^+. Chupka and Russell[25] reported more than 10 years ago that the $^2P_{1/2}$ state reacts with H_2 about 1.3 times faster than the $^2P_{3/2}$ state at nominally zero kinetic energy, as indirectly deduced from their photoionization intensity measurements. The agreement between their (1.3) and our (1.5) results is rather marvelous considering that the Chupka and Russell value was obtained using a single ionization chamber where three reactions, $Ar^+(^2P_{3/2})+H_2$, $Ar^+(^2P_{1/2})+H_2$, and $H_2^+ + Ar$, contributed to the measured ArH^+ intensity.

On the other hand, Rakshit and Warneck[26] recently reported that the major process of $Ar^+(^2P_{1/2})$ in H_2 is the quenching to the $Ar^+(^2P_{3/2})$ ground state and that the rearrangement reaction to form ArH^+ is about two orders of magnitude slower for $Ar^+(^2P_{1/2})$ than for $Ar^+(^2P_{3/2})$. This obviously contradicts our and Chupka and Russell results.

In order to confirm the enhanced reactivity of the $^2P_{1/2}$ state as compared with the $^2P_{3/2}$ state, and also to provide a rough idea about the relative magnitudes of the cross sections for Reactions (1) and (2) in a clearer way, we have also measured the photoionization efficiency curves (PIEC) of the relevant species using double chambers. These are shown in Fig. 4, together with a threshold electron spectrum of Ar (top diagram). The curve labeled $(Ar^+)_0$ is a PIEC of Ar taken without H_2 in the reaction chamber (Ar in the ionization chamber). When H_2 is introduced into the reaction chamber, this curve is reduced to that labeled Ar^+ and instead curves of ArH^+ and H_2^+ appear. What is remarkable here is that a stepwise decrease in the Ar^+ efficiency and a stepwise increase in the ArH^+ and H_2^+ efficiencies are clearly seen at the threshold of $Ar^+(^2P_{1/2})$, in spite of the much smaller production rate of $Ar^+(^2P_{1/2})$ than that of $Ar^+(^2P_{3/2})$ at and above this threshold. This undeniably demonstrates the enhanced reactivity of the $^2P_{1/2}$ state in both Reactions (1) and (2). These steps were not observed in the single chamber experiments of Chupka and Russell,[25] presumably owing to the obscuration by simultaneous occurrence of the $H_2^+ + Ar$ reaction.

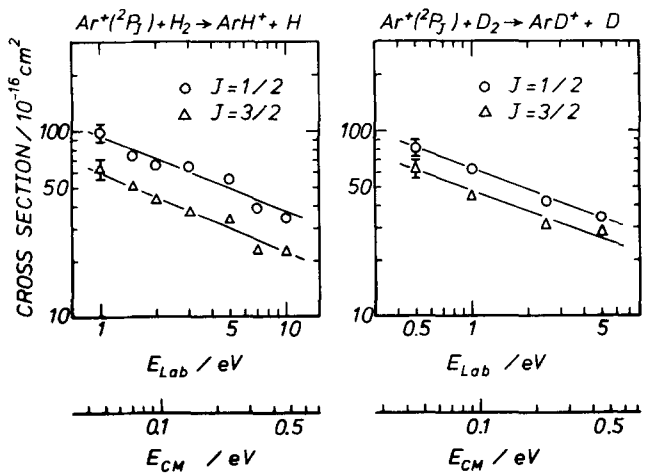

FIG. 3. State selected cross sections for Reaction (1) for the $^2P_{3/2}$ and $^2P_{1/2}$ states of Ar^+, as a function of collision energy.

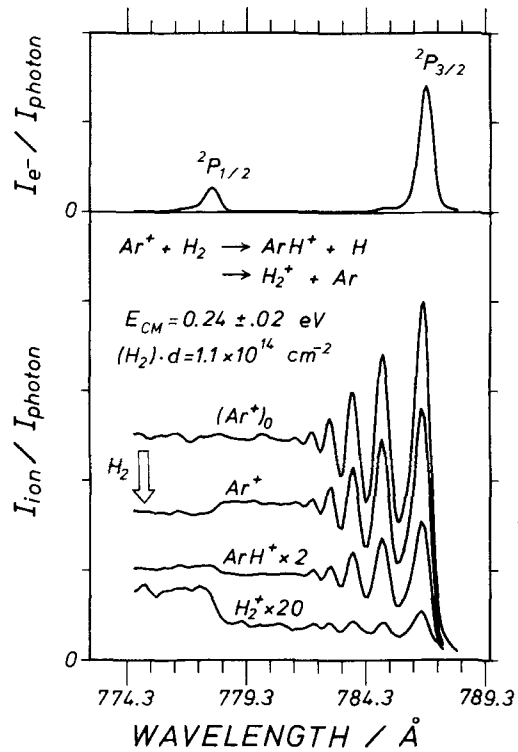

FIG. 4. Threshold electron spectrum of Ar (top) and photoionization efficiency curves for Ar^+ (with and without H_2 in the reaction chamber), ArH^+, and H_2^+, taken with double chambers. The number density of H_2 in the reaction chamber is indicated in terms of $(H_2)\cdot d$, where $d = 0.6$ cm.

These steps definitely refute the validity of the Rakshit and Warneck interpretation[26] of their experimental results: If the quenching to the $^2P_{3/2}$ ground state were the major process of the $Ar^+(^2P_{1/2})+H_2$ interaction and the reaction (1) with $Ar^+(^2P_{1/2})$ were much slower than that with $Ar^+(^2P_{3/2})$ as they insist, the down step in the Ar^+ efficiency and the up step in the ArH^+ efficiency could not occur at the $^2P_{1/2}$ threshold.

Figure 4 also clearly shows, qualitatively at least,

that the enhancing effect by the $^2P_{1/2}$ state is larger for Reaction (2) than for Reaction (1), and that the cross section for Reaction (2) is less than 5% of that for Reaction (1) with $^2P_{3/2}$ and somewhat higher with $^2P_{1/2}$, in agreement with the quantitative studies given above and in the next part (see Sec. IIIC). It is also seen that the fraction of the primary ions lost by scattering and/or product ions which escaped detection is about 20%–25%.

Concerning the magnitude and energy dependence of the cross section or rate constant, considerable disagreement remains among existing literatures. Our collision energy dependence of the cross sections described above gives rate constants of Reaction (1) which increase with collision velocity, in contrast with the expectation from the simple Langevin theory, as shown in Figs. 5 and 6. In this context, our results agree with the previous flowing afterglow (FA),[20] trapped-ion mass spectrometer,[12] guided-beam tandem mass spectrometer (GBTMS),[14] and ICR[21] studies. However, the ICR result[21(a)] shows a weakly discernible maximum of the rate constant around 0.2 eV (c.m.) and a gradual decrease above that energy (in the D_2 reaction), in disagreement with our result which shows the rate constant increasing up to 0.5 eV (c.m.). The latter result is supported by the GBTMS experiment[14] which reports that the rate constant increases up to ~0.7 eV (c.m.) collision energy and then begins to decrease. Moreover, the rate of increase in the energy range 0.05–0.5 eV (c.m.) agrees quite well between our and the GBTMS experiments. The temperature dependence of the rate constant of the FA experiment, on the other hand, gives almost the same gradient (as a function of average collision velocity) in the D_2 reaction but gives much steeper gradient in the H_2 reaction (although the average collision velocity range covered by the FA experiment falls below that covered by our experiment). Anyhow, all of these experiments indicate the occurrence of a small activation energy in this rearrangement channel.

As to the magnitudes of the rate constant, our result gives higher values than those obtained in the GBTMS and ICR experiments at all energies. The FA rate constant for both the H_2 and D_2 reactions (the lowest-pressure value) overlaps that of ours within the experimental error at 500 K (average collision velocity = 2.4×10^5 cm/s for H_2 and 1.7×10^5 cm/s for D_2).

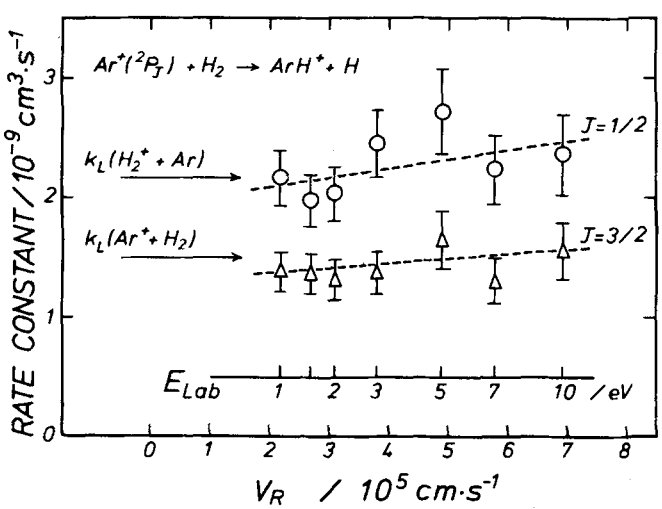

FIG. 5. State selected rate constant for Reaction (1) (with H_2) as a function of collision velocity. k_L indicates the Langevin rate constant for the system specified in the parenthesis.

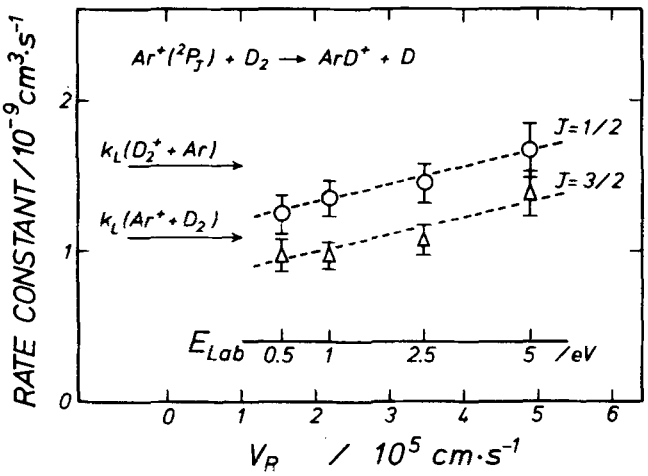

FIG. 6. State selected rate constant for Reaction (1) (with D_2) as a function of collision velocity. k_L indicates the Langevin rate constant for the system specified in the parenthesis.

Teloy and Gerlich[14] noted that theirs and the FA values at low energies are smaller than those from most of the previous conventional mass spectrometric measurements (the latter are almost "Langevin") by typically 25%, and tentatively attributed this discrepancy to the possible difference in the relative abundance of excited Ar^+ ions in the reactant. However, the state selected rate constants in the present study show that this can not be the reason for the low absolute values, since the pure $^2P_{3/2}$ state gives rate constants which are almost Langevin and the $^2P_{1/2}$ state gives higher values. In Figs. 5 and 6, the Langevin rate constants are indicated by horizontal arrows labeled k_L for each system specified in the parenthesis. It is seen that the experimental rate constants for the $^2P_{1/2}$ excited state are rather close to the Langevin value for the $H_2^+(D_2^+)$ + Ar system which is larger than that for the $Ar^+ + H_2(D_2)$ system because of the larger polarizability of Ar than that of H_2. Thus, the low rate constants of the FA and GBTMS experiments may need to seek explanation elsewhere.

Considering the nature of the potential energy surface of the $(Ar-H-H)^+$ system shown in the next section (Sec. IV), we would like to emphasize that what should actually be compared with experiment is the Langevin value for the $H_2^+(D_2^+)$ + Ar system, rather than that for the $Ar^+ + H_2(D_2)$ system. In fact, our model calculation using the Langevin-type barrier on the H_2^+ + Ar adiabatic potential surface gives results in good agreement with the experiment (see Sec. IV).

C. State selected cross sections for the charge transfer channel

1. *Determination of cross sections*

As stated in the experimental section, the very weak intensity of the charge transfer product (less than 10%

of the rearrangement product) rendered the coincidence measurements of it impractical. Thus the charge transfer cross sections were determined utilizing conventional pressure studies carried out at two wavelengths, 786.5 and 584 Å. An example of such pressure studies (for the H_2 reaction) is shown in Fig. 7. In these experiments, a weak potential gradient was applied between the ion inlet and ion outlet of the reaction chamber to confirm complete collection of the charge transfer product. This gives the uncertainty of the collision energy E shown in the figure.

At 786.5 Å, the primary ions produced consist entirely of $Ar^+(^2P_{3/2})$ and thus cross sections for this state can be determined without using the coincidence technique for both Reactions (1) and (2). However, we obtained from these measurements only the relative values of the charge transfer cross sections with respect to the rearrangement cross sections, and converted them to absolute values using the absolute cross sections for the latter reaction determined above using the coincidence technique. The charge transfer cross sections for the $^2P_{1/2}$ state, on the other hand, were determined from the similar relative cross sections obtained in the 584 Å experiments with the knowledge of the rearrangement cross sections, for both $^2P_{3/2}$ and $^2P_{1/2}$, and the charge transfer cross sections for $^2P_{3/2}$ obtained above. Here it was assumed that the reactant ions were produced in the $^2P_{3/2}$ and $^2P_{1/2}$ states in the 2:1 statistical ratio at 584 Å.

It is immediately evident from Fig. 7 that the relative intensity of the H_2^+ ion with respect to the Ar^+ intensity is increased considerably in going from 786.5 to 584 Å, whereas the increase in the relative intensity of the ArH^+ ion is not so significant. This prominent increase in the charge transfer product was not seen in the D_2 reaction.

2. Results and discussion

Results for the charge transfer channel are summarized in Fig. 8. Because the charge transfer data were

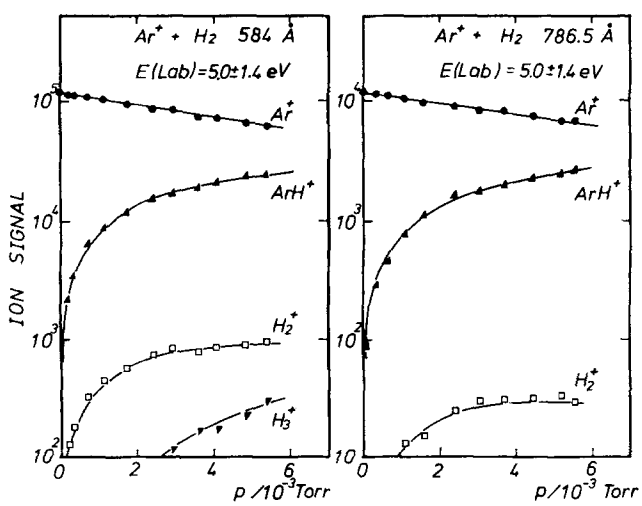

FIG. 7. Pressure plot of the primary and secondary ions of Reactions (1) and (2), obtained at two different wavelengths.

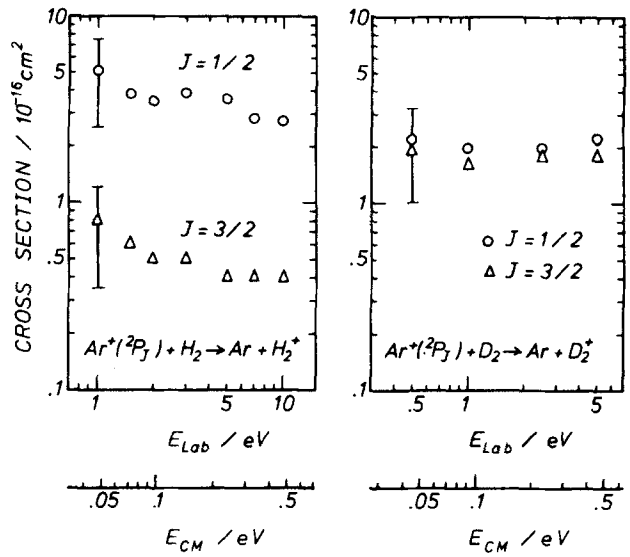

FIG. 8. State selected cross sections for Reaction (2) for the $^2P_{3/2}$ and $^2P_{1/2}$ states of Ar^+, as a function of collision energy.

obtained without coincidence, and also because of the long error bars (indicated in the figure), we consider these results as preliminary, especially concerning the absolute values of the cross sections. Nevertheless some interesting features are clearly noted: First, the cross sections for the $^2P_{1/2}$ state are about seven times larger than those for the $^2P_{3/2}$ state in the H_2 reaction, whereas these are almost the same for both states in the D_2 reaction, the values in the D_2 reaction falling between the two values in the H_2 reaction. Also, there seems to be subtle difference between the H_2 and D_2 reactions concerning the collision energy dependence of the cross section: The slight increase in the cross section with decreasing collision energy observed in the H_2 reaction is not seen in the D_2 reaction.

The rather large difference in the cross sections for H_2 between the $^2P_{1/2}$ and $^2P_{3/2}$ states presumably results from the enhanced cross section for the former state due to the energy resonance of the $v=2$ level of H_2^+ and the $^2P_{1/2}$ state of Ar^+ (0.016 eV endoergic, see Fig. 11). No level of H_2^+ is in such resonance with the $^2P_{3/2}$ state and no levels of D_2^+ lie so close to either state of Ar^+.

The importance of energy resonance in charge transfer processes has often been mentioned in the literature but has not yet been fully established. The kinematic study by Hierl *et al.*[23] on Reaction (2) has shown that the two distinct mechanisms are operative in this system at low collision energies: A simple electron jump mechanism and an intimate-collision mechanism. For the former mechanism they found that the translational energy distribution of products is best explained by a model which assumes selective production of H_2^+ in the vibrational state most nearly resonant with the reactant ion. Although their results do not give any information on the absolute values of the cross section, our present results presumably indicate that the actual magnitude of cross section is largely dependent on how close this most nearly resonant state lies to the reactant state. Hierl *et al.* compared their observed product transla-

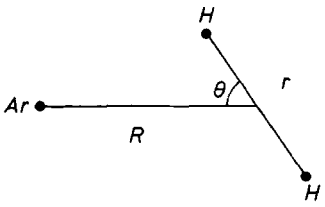

FIG. 9. The coordinate system used.

tional energy distribution with that expected from the electron jump model based on the assumption that the two states of Ar^+, $^2P_{3/2}$ and $^2P_{1/2}$, have equal charge transfer cross sections. However, their experimental results seem to be explained equally well (or even better) with the cross section ratio observed here.

Figure 8 shows that the charge transfer cross section ratio is almost independent of the collision energy in the range 0.05–0.5 eV (c.m.). This may imply that the close resonance between the reactant and product states plays an important role as well in the intimate-collision mechanism, since otherwise the enhanced nature of the $^2P_{1/2}$ state would have been reduced greatly at low collision energies (e.g., 0.1 eV) where the proportion of the intimate-collision mechanism is increased considerably compared with that at higher collision energies (e.g., 0.5 eV).[23]

IV. REACTION MODEL AND CALCULATION OF CROSS SECTIONS

In order to understand the experimental results presented in Sec. III, we have developed a simple reaction model and performed a model calculation of reaction cross sections to see whether the observed cross section ratio $\sigma(1/2)/\sigma(3/2)$ and its collision energy dependence and isotope effect can be reproduced or not. These are presented in this section. The coordinate system used in the following discussion is shown in Fig. 9.

A. The model

As stated in the introductory section, the $(Ar-H-H)^+$ system is characterized by the fact that, of the three

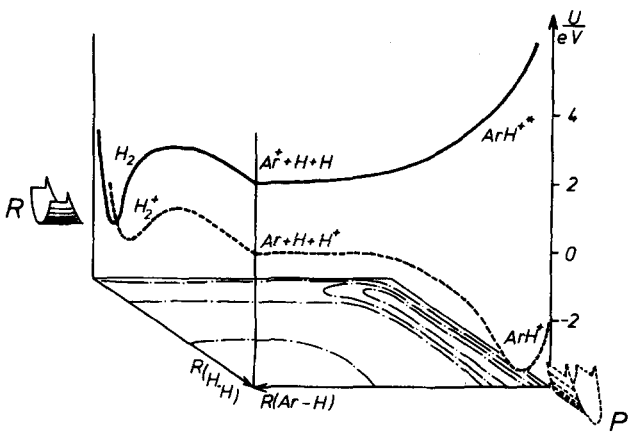

FIG. 10. Two asymptotic cuts ($R=\infty$ and $r=\infty$) of the two lowest potential energy surfaces for the $(Ar+H+H)^+$ system. An equipotential plot of the lowest surface is also shown on the bottom of the box.

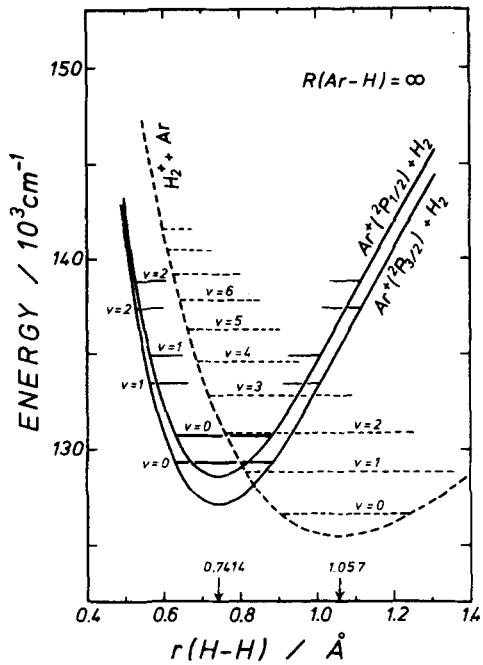

FIG. 11. The $R=\infty$ asymptote of the four low-lying potential energy surfaces of the $(Ar+H+H)^+$ system, with spin-orbit interaction being included.

atom + diatom ground state channels, only $Ar^+ + H_2$ correlates to $Ar^+ + H + H$ fragments, whereas $Ar + H_2^+$ and $ArH^+ + H$ correlate to $Ar + H^+ + H$. This means that the system $Ar^+ + H_2$ is nonreactive in a totally diabatic picture and requires mixing and consequent nonadiabatic transitions between two surfaces in order for the rearrangement (forming $ArH^+ + H$) or charge transfer (forming $H_2^+ + Ar$) to occur. This situation is visualized in Fig. 10 which schematically shows the two asymptotic sections ($R=\infty$ and $r=\infty$) of the two relevant potential energy surfaces (an equipotential plot of the lowest energy surface is also shown on the bottom of the box). These and other features of six low-lying potential energy surfaces (without spin–orbit coupling) have well been established by the DIMZO (diatomics-in-molecule with zero overlap) technique.[2,3]

When spin–orbit coupling is taken into account, the entrance ($R=\infty$) asymptotes of the four lowest-lying potential energy surfaces are like that shown in Fig. 11. The separation of the two solid line curves is, of course, the spin–orbit coupling separation for the free Ar^+ ion (178 meV), and the lower solid line curve labeled $Ar^+(^2P_{3/2}) + H_2$ actually represents two states $Ar^+(^2P_{3/2,1/2}) + H_2$ and $Ar^+(^2P_{3/2,3/2}) + H_2$, which have the same energy at $R=\infty$ and in the absence of external field (the subscripts mean J and M_J with M_J quantization along **R**). Thus, these four low-lying states are

(i) $Ar + H_2^+(X^2\Sigma_g^+)$, (broken line curve),

(ii) $Ar^+(^2P_{3/2,1/2}) + H_2$,

(iii) $Ar^+(^2P_{3/2,3/2}) + H_2$,

(iv) $Ar^+(^2P_{1/2,1/2}) + H_2$.

The spin–orbit Hamiltonian H_{so} mixes the Σ and Π states which originate from the $Ar^+(^2P) + H_2$ interaction

and the mixing coefficients are given by the Clebsch–Gordon coefficients.[29] Further, in the general C_s configuration (for $\theta \neq 0$, Fig. 9), the π orbitals are split into two classes, those having a' and a'' symmetry, whereas σ orbitals have a' symmetry (these are denoted as $3p\pi a'$, $3p\pi a''$, and $3p\sigma a'$, respectively). At large distances the wave functions of states (ii)–(iv) may be expressed in terms of the Ar spin–orbital vacancy (with respect to the closed-shell system $Ar + H_2$) in point group C_s as

$$\text{(ii)} \begin{cases} \frac{\sqrt{6}}{6}(\overline{3p\pi a'} + i\,\overline{3p\pi a''}) + \frac{\sqrt{6}}{3} 3p\sigma a' \,, \\ \frac{\sqrt{6}}{6}(3p\pi a' - i\,3p\pi a'') + \frac{\sqrt{6}}{3}\overline{3p\sigma a'} \,, \end{cases}$$

$$\text{(iii)} \begin{cases} \frac{\sqrt{2}}{2}(3p\pi a' + i\,3p\pi a'') \,, \\ \frac{\sqrt{2}}{2}(\overline{3p\pi a'} - i\,\overline{3p\pi a''}) \,, \end{cases}$$

$$\text{(iv)} \begin{cases} \frac{\sqrt{3}}{3}(\overline{3p\pi a'} + i\,\overline{3p\pi a''} - 3p\sigma a') \,, \\ \frac{\sqrt{3}}{3}(3p\pi a' - i\,3p\pi a'' - \overline{3p\sigma a'}) \,. \end{cases}$$

Similarly, the charge transfer state (i) is defined by a vacancy in the H_2 spin–orbital as

$$\text{(i)} \begin{cases} \sigma_g a' \\ \overline{\sigma_g a'} \end{cases} .$$

When the reactants approach each other (namely, R is reduced from infinity), states (ii)–(iv) are mixed by the electrostatic Hamiltonian H_{el}, the extent of mixing of each state depending on R. This mixing is primary connected with the $3p\sigma$–$3p\pi$ splitting and, to a minor extent, with the $3p\pi a'$–$3p\pi a''$ splitting in the C_s case.

With the above general features of the system in mind, we assume in our model that the reaction cross sections for $Ar^+(^2P_{3/2})$ and $Ar^+(^2P_{1/2})$ are, respectively, proportional to the transition probability from states (ii)/(iii) to state (i) and that from state (iv) to state (i). It is assumed that the rearrangement channel takes place only when the system $Ar^+ + H_2$ approaching with impact parameter b smaller than b_0 (velocity dependent) undergoes transition. The critical impact parameter b_0 is obtained from the Langevin-type calculation using the lowest adiabatic potential energy surface of the $(Ar + H + H)^+$ system. Thus, the essential part of our model calculation is to work out the mixing of states (ii)–(iv) as a function of R and thereafter calculate their couplings with state (i) [transition probabilities to state (i)].

B. Coupling of the $Ar^+ + H_2$ states with the $Ar + H_2^+$ state

We now consider the coupling by H_{el} of states (ii)–(iv) with state (i). From the calculations of Chapman and Preston[3] we learn that, among the diabatic states designated in Sec. IV A as $3p\sigma a'$, $3p\pi a'$, and $3p\pi a''$, only $3p\sigma a'$ is significantly coupled with $\sigma_g a'$. The $3p\pi a'$ state is not coupled with $\sigma_g a'$ when $\theta = 0°$ or 90°, and their coupling at other angles, as exemplified by $\theta = 45°$, is too small for giving rise to actual transitions.[3] Finally, the $3p\pi a''$ state is not coupled at all with $\sigma_g a'$ by H_{el} because of their different symmetries in the (most general) C_s point group. In the above statements our $\sigma_g a'$, $3p\sigma a'$, and $3p\pi a'$ states would correspond after diagonalization of the electrostatic Hamiltonian to Chapman and Preston's E_1, E_2, and E_3 states.[3]

From the above discussion it turns out that the coupling between each of the states (ii)–(iv) and state (i) will be dependent only on the $\sigma_g a'$ content of each of the former states. In the first approximation, in which mixing of states (ii)–(iv) is not considered, these contents are

$$\begin{aligned} &\langle \sigma_g a' | \text{(ii)} \rangle = \sqrt{6}/3 \,, \\ &\langle \sigma_g a' | \text{(iii)} \rangle = 0 \,, \\ &\langle \sigma_g a' | \text{(iv)} \rangle = -\sqrt{3}/3 \,, \end{aligned} \tag{12}$$

as deduced using the wave functions (ii)–(iv) given above.

Now we mix the states (ii)–(iv) as a second approximation. As stated above, the mixing is caused by $3p\sigma$–$3p\pi$ and $3p\pi a'$–$3p\pi a''$ splittings which occur as R is decreased. These energy separations are denoted as $\Delta(R)$ and $\delta(R)$, respectively. Spin–orbit separation between states (ii)/(iii) and (iv), on the other hand, is assumed to be independent of R and equal to the value for $R = \infty$ (0.178 eV). This value is denoted as A. At comparatively large R, the order of increasing magnitude of these values is δ, Δ, A.

The Hamiltonian matrix elements for states (ii)–(iv) are computed in terms of $\Delta(R)$, $\delta(R)$, and A and the matrix is then diagonalized. Using new wave functions (ii)′, (iii)′, and (iv)′ obtained by diagonalization (see Appendix B), we compute the $\sigma_g a'$ component $\langle \sigma_g a' | (j)' \rangle$ of these new states [j = (ii)–(iv)], knowing the values $\langle \sigma_g a' | (j) \rangle$ [Eq. (12)]. These procedures finally give the following coupling matrix elements H_{12}^j between the Ar + H_2^+ state and each state of $Ar^+ + H_2$, to the first order in δ/Δ and δ/A:

$$\begin{aligned} H_{12}^{ii} &= \langle Ar^+(^2P_{3/2,1/2}) + H_2 | H_{el} | Ar + H_2^+ \rangle = \left[\frac{\sqrt{3}}{3}(1+X)^{1/2} + \frac{\sqrt{6}}{6}(1-X)^{1/2}\right] H'_{12} \,, \\ H_{12}^{iii} &= \langle Ar^+(^2P_{3/2,3/2}) + H_2 | H_{el} | Ar + H_2^+ \rangle = -\frac{\sqrt{2}}{4}\frac{\delta}{\Delta} H'_{12} \,, \\ H_{12}^{iv} &= \langle Ar^+(^2P_{1/2,1/2}) + H_2 | H_{el} | Ar + H_2^+ \rangle = \left[-\frac{\sqrt{6}}{6}(1+X)^{1/2} + \frac{\sqrt{3}}{3}(1-X)^{1/2}\right] H'_{12} \,, \end{aligned} \tag{13}$$

TABLE I. Comparison of the cross section ratio $\sigma(1/2)/\sigma(3/2)$.

$Ar^+(^2P_J)+H_2 \rightarrow ArH^+ + H$			$Ar^+(^2P_J)+D_2 \rightarrow ArD^+ + D$		
	$\sigma(1/2)/\sigma(3/2)$			$\sigma(1/2)/\sigma(3/2)$	
E_{CM} (eV)[a]	(Exptl.)	(Model)	E_{CM} (eV)[a]	(Exptl.)	(Model)
0.05±0.03	1.59	1.29	0.05±0.02	1.29	1.50
0.10±0.04	1.53	1.27	0.09±0.02	1.38	1.49
0.24±0.07	1.65	1.29	0.23±0.03	1.35	1.50
0.48±0.09	1.48	1.32	0.46±0.05	1.21	1.56

[a]The uncertainty in E_{CM} is mainly due to the thermal motion of target molecules.

where

$$X = \frac{A + \Delta/3}{(A^2 + 2A\Delta/3 + \Delta^2)^{1/2}} \tag{14}$$

and H'_{12} is the coupling matrix element between the $Ar^+ + H_2$ and $Ar + H_2^+$ states without spin–orbit coupling.

These coupling matrix elements are used in the calculation of Landau–Zener transition probabilities as H_{12} (see below).

C. Computation of transition probabilities and reaction cross sections

The probability for a single transition from a state correlated with $Ar^+ + H_2$ (state 1) to the state correlated with $Ar + H_2^+$ (state 2) is calculated according to the Landau–Zener equation

$$P_{12} = 1 - \exp\left(-2\pi H_{12}^2 \Big/ \hbar v_r \left|\frac{\partial H_{22}}{\partial r} - \frac{\partial H_{11}}{\partial r}\right|\right).$$

Here, v_r is the velocity along the r coordinate, and is derived from the classical kinetic energy of vibration (transition is known to be caused by vibrational motion of H_2, see Sec. I). H'_{12}, which is necessary to calculate H_{12}, is obtained by the analytical fit of Baer and Beswick's coupling term [Fig. 2 of Ref. 4(c)] as

$$H'_{12} = 33.2 \exp(-1.15R), \tag{15}$$

where R is in Å and H'_{12} in eV. H_{11} and H_{12} are assumed to be independent of R and taken as the potential curves of H_2^+ (+Ar) and H_2 (+Ar^+) at infinite R.

The total transition probabilities P_0 for a collision with a given impact parameter b and a velocity v are obtained by integrating the R-dependent Landau–Zener probability from $R=\infty$ to $R=R_0$, where R_0 is the distance of closest approach for the given b and v (P_0 is always computed on the $Ar^+ + H_2$ potential and thus the R_0 is the distance of closest approach on this potential). The Landau–Zener probabilities are raised to the power of $2dt/T$ to allow for the number of passages of the $Ar^+ + H_2$ system by the crossing point during the time element dt, where $T/2$ is a half period of vibration of H_2. T is also assumed to be independent of R and the value at infinite R is used.

Using the total transition probabilities $P_0(b)$ obtained above, reaction cross sections σ_r are computed according to the equation

$$\sigma_r = \int_0^{b_0} 2\pi b\, db P_0(b), \tag{16}$$

where b_0 is the critical impact parameter described in Sec. IV A. The model assumes, as can be seen from Eq. (16), that if the system undergoes transition from the initial diabatic state ($Ar^+ + H_2$) at least once in the trajectory between ∞ and R_0, it is considered eventually to be on the adiabatic surface connected with the $ArH^+ + H$ products. Equation (16) also implies that in order for the reaction to take place, the system still has to overcome the Langevin-type centrifugal barrier of the adiabatic surface to which it has undergone transition. This adiabatic surface, used in the calculations of b_0, is obtained in the following manner: First, two diabatic potentials $V_{Ar^+ + H_2}$ and $V_{Ar + H_2^+}$ are constructed by adding polarization terms to the analytical DIM potentials of Baer and Beswick.[4(c)] These are then diagonalized using the coupling term H'_{12} described above.

D. Results and discussion

Results of the calculation are given in Table I and Fig. 12. Table I compares the theoretical and experimental ratios of the cross sections for $J=\frac{3}{2}$ and $J=\frac{1}{2}$. It is seen that, in spite of many assumptions and approximations taken in the theory, the essential features of the rearrangement channel are reproduced in the present calculation. Namely, the rearrangement cross section is definitely larger for $J=\frac{1}{2}$ than for $J=\frac{3}{2}$ and their ratio falls roughly between 1.3 and 1.5, independent of the collision energy. One point which is apparently not satisfactory is the reverse isotope effect obtained in the calculation: The ratio is somewhat larger for D_2 reactions than for H_2 reactions, contrary to the experimental result.

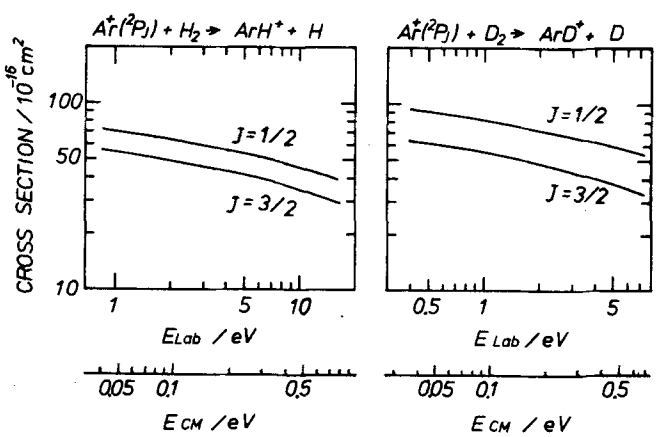

FIG. 12. State selected cross sections for Reaction (1) calculated based on the model.

Figure 12 shows that the experimental absolute cross sections and their collision energy dependence are also fairly satisfactorily reproduced by the present theory (cf. Fig. 3). It is noted, however, that the theory tends to give cross sections which are somewhat higher than the experiment at higher collision energies and the reverse at lower collision energies. This naturally gives somewhat milder collision energy dependence than the experiment: Fig. 12 yields the $E^{-1/3}$–$E^{-1/4}$ dependence, in contrast with the experimental $\sim E^{-1/2.5}$ dependence.

All of the above discrepancies are probably due, partly, at least, to some crude assumption(s) and approximation(s) used in the theory and may certainly be improved by reexamining and refining these assumptions and approximations. In spite of these discrepancies, the general agreement obtained above seems to indicate that the present model is much to the point of what is happening in this reaction system.

We have also performed calculations for the charge transfer channel. In this case, however, additional assumptions and unknown factors make the situation more complicated. A factor which is most difficult to estimate is the branching ratio between the charge transfer ($Ar + H_2^+$) and scattering ($Ar^+ + H_2$) channels for the system which undergoes transition outside b_0 and in the outgoing phase of the trajectory which lies inside b_0. In fact, this branching ratio might rather be derived from our experimental results than estimated *a priori*.

V. SUMMARY AND CONCLUDING REMARKS

We have determined the reaction cross sections for $Ar^+ + H_2(D_2) \rightarrow ArH^+(ArD^+) + H(D)$ and $Ar^+ + H_2(D_2) \rightarrow Ar + H_2^+(D_2^+)$ for each of the reactant spin–orbit states ($^2P_{3/2}$ and $^2P_{1/2}$) separately, as a function of collision energy. It has been shown that the atomic rearrangement reaction takes place about 1.5 times faster (with H_2) and 1.3 times faster (with D_2) for the $^2P_{1/2}$ excited state than for the $^2P_{3/2}$ ground state, regardless of the collision energy in the range 0.05–0.5 eV (c.m.). The cross sections for both H_2 and D_2 reactions show collision energy dependence which is somewhat less steep than that expected from the simple Langevin theory, indicating the occurrence of small activation energy.

As to the charge transfer reaction, cross sections are about seven times larger for the $^2P_{1/2}$ state than for the $^2P_{3/2}$ state in the H_2 reaction, whereas they are almost the same for both states in the D_2 reaction, again regardless of the collision energy.

These main features of the experimental results have been found to be explained satisfactorily by a simple reaction model, essential part of which consists of mixing of three states originating from the $Ar^+ + H_2$ interaction (taking the spin–orbit interaction into account) and subsequent transitions from each of these new states to the $Ar + H_2^+$ state.

The enhancement of ion–molecule reaction cross sections when there is a quasiresonance between the initial state and a charge–transfer state was pointed out long ago[30] and was explained as due to the lowering of the Langevin barrier as a result of repulsion of potential surfaces around an avoided crossing between the entrance and charge–transfer states. The same idea was used by Gislason[31] (about the $Ar^+ + H_2$ reaction) and by Yencha *et al.*[32] with the additional contention that resonances between specific vibronic levels have to be considered. In particular, $Ar^+(^2P_{1/2}) + H_2\ (v=0)$ is almost resonant with $Ar + H_2^+\ (v=2)$ which lies only 16 meV higher. One of the aims of the present work was to test whether avoided crossing effects have to be considered for specific vibronic potential curves or simply for potential hypersurfaces. The comparison between $Ar^+ + H_2$ and $Ar^+ + D_2$ (where no resonances between vibronic levels occur for any fine-structure state) was an obvious test first suggested by Chupka.[33]

Our results appear to contradict the idea of vibrational specificity of curve-crossing effects: The reaction cross section is larger for $^2P_{1/2}$ than for $^2P_{3/2}$ as well in the D_2 as in the H_2 reaction, although the cross section ratio is larger with H_2 than with D_2. Moreover, the collision energy dependence of the cross sections is identical for both fine-structure states, showing that their locations with respect to the vibronic levels of the charge–transfer state are of little importance in the reaction dynamics. Finally, the fact that the main features of our experimental results are conveniently described by the simple model we developed, where no account is taken of the H_2 (or H_2^+) vibrational quantization, also points to the same conclusion. More recent results on the reaction of H_2^+ in specific vibrational levels with Ar confirm that vibronic resonance effects are of minor importance for the rearrangement reactions.[34] In contrast, these effects are dramatic as regards the charge transfer reactions, as well for $Ar^+ + H_2(D_2) \rightarrow H_2^+(D_2^+) + Ar$ (present results) as for the reverse reaction.[34]

Our conclusion that the quantization of the H–H motion (r coordinate) has no effect on the dynamics of the reactive collisions in the Ar^+/H_2 system seems to contradict the theoretical results of Baer and Beswick,[4(c)] according to whom the H_2 vibration is still behaving adiabatically at the distances R where the transition from states (ii)/(iv) to state (i) takes place. However, the calculations of these authors were limited to collinear geometry and therefore neglected any coupling of the r motion with the bending motion as well as with the overall rotation.

APPENDIX A: DERIVATION OF EQ. (9)

Referring to Reactions (1)–(7) and putting $\sigma \equiv \sigma_r + \sigma_t + \sigma_s$ and $\sigma' \equiv \sigma'_r + \sigma'_s$, the rate equations for Ar^+ and ArH^+ are

$$\frac{d[Ar^+]}{dx} = -\sigma[Ar^+]n\ , \tag{17}$$

$$\frac{d[ArH^+]}{dx} = \sigma_r[Ar^+]n - \sigma'[ArH^+]n\ , \tag{18}$$

where n is the number density of $H_2(D_2)$. Solutions of these equations at $x=d$ (≡ reaction path length in the reaction chamber) multiplied by the respective collecting efficiencies, λ and λ', give the expression for the measured intensities of Ar^+ and ArH^+ as follows:

$$(Ar^+) = \lambda[Ar^+]_0 \exp(-\sigma nd) , \tag{19}$$

$$(ArH^+) = \lambda'\sigma_r[Ar^+]_0 \frac{\exp(-\sigma' nd) - \exp(-\sigma nd)}{\sigma - \sigma'} , \tag{20}$$

where $[Ar^+]_0$ is the Ar^+ density at the entrance of the reaction chamber. Thus, we obtain

$$\frac{(ArH^+)}{(Ar^+)} = \frac{\lambda'}{\lambda} \cdot \frac{\sigma_r}{\sigma - \sigma'} \{\exp[(\sigma - \sigma')nd] - 1\} . \tag{21}$$

On the other hand, the variation of (Ar^+) and (ArH^+) with pressure gives

$$\frac{d(Ar^+)}{d(ArH^+)} = -\frac{\lambda}{\lambda'} \cdot \frac{\sigma - \sigma'}{\sigma_r} \cdot \frac{\sigma}{\sigma - \sigma' \exp[(\sigma - \sigma')nd]} . \tag{22}$$

Under the condition $\sigma' nd \ll 1$, i.e., in the limit of $n \to 0$, the right side of Eq. (22) is reduced to $-(\lambda/\lambda')(\sigma/\sigma_r) = -(\lambda/\lambda')[1 + (\sigma_t + \sigma_s)/\sigma_r]$. This constant is denoted by m [Eq. (10)]. On the other hand, from Eqs. (21) and (22) it is seen that at the density n which gives $d[ArH^+]/d[Ar^+] = 0$, the ratio $[Ar^+]/[ArH^+]$ becomes $(\lambda/\lambda')(\sigma'/\sigma_r) = (\lambda/\lambda')[(\sigma'_r + \sigma'_s)/\sigma_r]$. This constant is denoted by q [Eq. (11)]. Rearranging Eq. (21) with these constants, we obtain Eq. (9).

APPENDIX B: HAMILTONIAN MATRIX FOR THE STATES (ii)-(iv) AND ITS DIAGONALIZATION

Under the assumptions given in Sec. IV B, the Hamiltonian matrix for the states (ii)–(iv) is computed in terms of δ, Δ, and A as follows:

	(ii)	(iii)	(iv)
(ii)	$-\frac{A}{3} - \frac{\Delta}{3}$	$-\frac{\sqrt{3}\delta}{6}$	$\frac{\sqrt{2}\Delta}{3}$
(iii)	$-\frac{\sqrt{3}}{6}\delta$	$-\frac{A}{3} + \frac{\Delta}{3}$	$-\frac{\sqrt{6}\delta}{6}$
(iv)	$\frac{\sqrt{2}\Delta}{3}$	$-\frac{\sqrt{6}}{6}\delta$	$\frac{2}{3}A$

Here the average point is taken as the zero of energies. Diagonalizing this matrix (to the first order in δ/Δ and δ/A), we obtain the following new wave functions, (ii)′–(iv)′ from which the coupling matrix elements H^j_{12} [Eqs. (13)] are computed:

$$(ii)' = \frac{\sqrt{2}}{2}(1+X)^{1/2}(ii) + \frac{2\delta}{Y - A + \Delta}\left[\frac{\sqrt{6}}{12}(1+X)^{1/2} - \frac{\sqrt{3}}{6}(1-X)^{1/2}\right](iii) - \frac{\sqrt{2}}{2}(1-X)^{1/2}(iv) ,$$

$$(iii)' = -\frac{\sqrt{3}(A-\Delta)\delta}{4A\Delta}(ii) + (iii) + \frac{\sqrt{6}\delta}{4A}(iv) ,$$

$$(iv)' = \frac{\sqrt{2}}{2}(1-X)^{1/2}(ii) - \frac{2\delta}{Y + A - \Delta}\left[\frac{\sqrt{3}}{6}(1+X)^{1/2} + \frac{\sqrt{6}}{12}(1-X)^{1/2}\right](iii) + \frac{\sqrt{2}}{2}(1+X)^{1/2}(iv) ,$$

where X is given by Eq. (14) and $Y = A^2 + 2A\Delta/3 + \Delta^2$.

[1] J. C. Tully, in *Dynamics of Molecular Collisions*, edited by W. H. Miller (Plenum, New York, 1976), Part B, Chap. 5; S. M. Child, in *Atom–Molecule Collisions: A Guide for Experimentalists*, edited by R. B. Bernstein (Plenum, New York, 1979), Chap. 7.

[2] P. J. Kuntz and A. C. Roach, J. Chem. Soc. Faraday Trans. 2 **68**, 259 (1972).

[3] S. Chapman and R. K. Preston, J. Chem. Phys. **60**, 650 (1974).

[4] (a) M. Baer, Mol. Phys. **35**, 1637 (1978); (b) M. Baer and J. A. Beswick, Chem. Phys. Lett. **51**, 360 (1977); (c) Phys. Rev. A **19**, 1559 (1979).

[5] K. Lacmann and A. Henglein, Ber. Bunsenges. Phys. Chem. **69**, 286 (1965).

[6] Z. Herman, J. Kerstetter, T. Rose, and R. Wolfgang, Discuss. Faraday Soc. **44**, 123 (1967).

[7] M. Chiang, E. A. Gislason, B. H. Mahan, C. W. Tsao, and A. S. Werner, J. Chem. Phys. **52**, 2698 (1970).

[8] P. Hierl, Z. Herman, and R. Wolfgang, J. Chem. Phys. **53**, 660 (1970).

[9] R. C. Amme and J. F. McIlwain, J. Chem. Phys. **45**, 1224 (1966).

[10] D. P. Stevenson and D. O. Schissler, J. Chem. Phys. **29**, 282 (1958).

[11] F. S. Klein and L. Friedman, J. Chem. Phys. **41**, 1789 (1964).

[12] K. R. Ryan and I. G. Graham, J. Chem. Phys. **59**, 4260 (1973).

[13] C. F. Giese and W. B. Maier II, J. Chem. Phys. **39**, 739 (1963).

[14] E. Teloy and D. Gerlich, Chem. Phys. **4**, 417 (1974).

[15] A. Henglein, K. Lacmann, and B. Knoll, J. Chem. Phys. **43**, 1048 (1965).

[16] L. D. Doverspike, R. L. Champion, and T. L. Bailey, J. Chem. Phys. **45**, 4385 (1966).

[17] A. Ding, K. Lacmann, and A. Henglein, Ber. Bunsenges. Phys. Chem. **71**, 596 (1967).

[18] R. D. Fink and J. S. King, J. Chem. Phys. **47**, 1857 (1967).

[19] P. M. Hierl, Z. Herman, and R. Wolfgang, J. Chem. Phys. **53**, 660 (1970).

[20] N. G. Adams, D. K. Bohme, D. B. Dunkin, and F. C. Fehsenfeld, J. Chem. Phys. **52**, 1951 (1970).

[21] (a) R. D. Smith, D. L. Smith, and J. H. Futrell, Int. J. Mass Spectrom. Ion Phys. **19**, 395 (1976); (b) R. P. Clow and J. H. Futrell, *ibid.* **8**, 119 (1972); (c) M. T. Bowers and D. D. Elleman, J. Chem. Phys. **51**, 4606 (1969).

[22] P. Mahadevan and G. D. Magnuson, Phys. Rev. **171**, 103 (1968).

[23] P. M. Hierl, V. Pačak, and Z. Herman, J. Chem. Phys. **67**, 2678 (1977).

[24] T. F. Moran and P. C. Cosby, J. Chem. Phys. **51**, 5724 (1969).

[25] W. A. Chupka and M. E. Russell, J. Chem. Phys. **49**, 5426 (1968).

[26] A. B. Rakshit and P. Warneck, J. Chem. Phys. **73**, 2673 (1980).

[27] K. Tanaka, J. Durup, T. Kato, and I. Koyano, J. Chem. Phys. **73**, 586 (1980).

[28] (a) K. Tanaka and I. Koyano, J. Chem. Phys. **69**, 3422 (1978). (b) I. Koyano and K. Tanaka, *ibid.* **72**, 4858 (1980).

[29] A detailed study of a similar system may be found, for example, in E. A. Gordeev, E. E. Nikitin, and A. I. Shushin, Mol. Phys. **33**, 1611 (1977).

[30] J. Durup, *Les Réactions entre ions positifs et molecules en phase gazeuse* (Gauthier-Villars, Paris, 1960), p. 31.

[31] E. A. Gislason, J. Chem. Phys. **57**, 3396 (1972).

[32] A. J. Yencha, A. Münzer, and A. Niehaus, in "Abstract of Contributed Papers," XIth International Conference on the Physics of Electronic and Atomic Collisions (Kyoto, 1979), p. 902.

[33] W. A. Chupka, in *Interactions Between Ions and Molecules*, edited by P. Ausloos (Plenum, New York, 1975), p. 249.

[34] K. Tanaka, T. Kato, and I. Koyano (to be published).